

Using CFD to Study Combustion and Steam Flow Distribution Effects on Reheater Tubes Operation

Esmaeil Poursaeidi¹

e-mail: epsaeidi@znu.ac.ir

Masoud Arablu

e-mail: arablu_m@yahoo.com

Mechanical Engineering Department,
Faculty of Engineering,
Zanjan University,
P.O. Box 45195-313, Zanjan,
Iran

The thickness measurements showed that boilers of the Shahid Rajaee power plant have a non-uniform thickness in some regions of the final reheater tubes after 80,000 h of operation. Experimental tests on areas such as thickness, hardness, metallography, and recorded temperature showed that high temperature erosion is the most obvious reason for thinning in these tubes. Therefore, two possible reasons for the non-uniform tube thinning (problems due to combustion and steam mal-distribution in the tubes) were explored. This paper presents simulations of combustion, flow distribution in reheater tubes, and heat exchange process in Pass 1 of the boiler using FLUENT software. Combustion simulation results showed temperature distribution and mass flux of combustion products are not uniform at the chamber outlet. But these non-uniformities are not proportional to the tubes' thickness non-uniformity; whereas, simulations showed steam is mal-distributed in the tubes so that steam maldistribution is proportional to the tubes' thickness non-uniformities. Because steam maldistribution was due to mal-feeding and offloading of headers (U-type headers), all possible ways of feeding and offloading of headers were studied, and the results showed that the H-type configuration has the most uniform flow distribution. [DOI: 10.1115/1.4004081]

Keywords: CFD simulation, combustion, flow mal-distribution

1 Introduction

For a number of fluidic devices in the chemical process and power plant industries such as shell-tube heat exchangers, tubular reactors, static mixers, fuel cell stacks, and boilers, flow distribution is always important because it has significant influences on overall performance of things such as rate of mass/heat transfer, conversion or choice of reaction, etc. [1,2]. Flow maldistribution is generally caused by poor design and imprecise fabrication of the distributor, which will generally increase back-mixing and decrease the driving force of mass/heat transfer. When the flow is distributed into parallel channels, the maximal flow rate ratio (ratio of the highest volume flow rate to the lowest one) could be as high as 4, if no measures have been taken for uniform flow distribution as shown by Lalot et al. [3]. Flow maldistribution with so high a maximal flow rate ratio would decrease the efficiency of a crossflow heat exchanger by 25%.

Introducing a flow distributor for uniform flow distribution will undoubtedly increase flow resistance. Therefore, minimizing energy dissipation emerges as an important goal of distributor design. The constructal distributors, which have a branched multi-scale structure, have handsomely solved the problem of minimizing energy dissipation for uniform flow distribution. Different constructal distributors with different configurations have been proposed in the literature [4–6] that can be fabricated by stereolithography with epoxy resin or metal powder. However, because the 3-D constructal flow distributors are costly to fabricate, only a few were really fabricated and evaluated [7,8]. Furthermore, due

to fabrication and geometrical limits, a few of distributors can be used in the huge instruments such as power plant boilers.

For small instruments, serpentine, parallel serpentine, and interdigitated channels can be used where the pressure drop is of a smaller magnitude. However, for larger instruments such as boilers and heat exchangers, these styles of configurations will quickly increase the pressure drop to be on the order of a few bars due to the flow turning losses in curvature channels. On the other hand, the parallel-channel configurations possess a clear advantage of simplicity and less pressure drop over the serpentine style. However, when using the parallel-channel configurations, there is a possibility of severe flow maldistribution problems; this reduces instrument performance. Under ideal conditions, the performance of tubes in parallel-channel configuration is simply the linear sum of the performance of tubes in unit row. However, this linear correlation is not achieved in practice because of non-uniform flow distribution. Some channels may be starved of steam, whereas others may have it in excess.

Flow distribution in the parallel-channel distributors depends on two main factors: The friction of the fluid against the internal surface of the channels and the momentum of the main fluid stream flowing into an intake manifold header. The friction and momentum effects work in opposite directions; the former tends to produce a pressure drop and the latter a pressure rise. Therefore, it is possible to obtain a uniform pressure distribution along the header axis by suitable adjustment of the flow and design parameters so that the pressure recovery due to flow branching balances the pressure losses due to friction. The uniform pressure distribution along the header axis causes uniform flow distribution in the channels (tubes). On the other hand, the arrangement of headers feeding and offloading affects the pressure distribution along the headers. There are several types of arrangements used in parallel-channel configuration, such as U-type, Z-type, H-type, etc.; flow distribution and pressure drop in these types of manifold

¹Author to whom correspondence should be addressed.

Contributed by the Fluids Engineering Division of ASME for publication in the JOURNAL OF FLUIDS ENGINEERING. Manuscript received December 20, 2009; final manuscript received April 4, 2011; published online June 7, 2011. Assoc. editor: Hassan Peerhossaini.

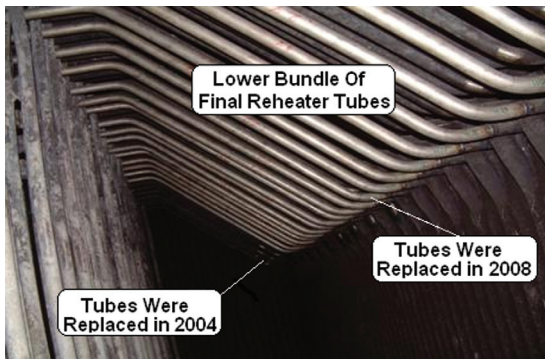


Fig. 1 Lower bundle of final reheat tubes

systems are a classic issue in chemical, mechanical, and civil engineering [6–13].

There are three approaches to study pressure drop and flow distribution in parallel-channel configurations: Computational fluid dynamics (CFD) [9–14], channel network models [15–18], and analytical models [14,19]. Recently, Junye Wang [20,21] has introduced an analytical model for evaluating the flow distribution in U- and Z-type configuration parallel channels. CFD is a somewhat detailed approach in which modeling has potential to resolve real-world 3-D engineering structures. The pressure drop and flow distribution can be predicted using this approach without the knowledge of flow coefficients, such as the friction and pressure recovery coefficients. But CFD is unsuitable for optimizing parallel-channel geometries and preliminary designs because it is too expensive to regenerate the computational geometry and mesh for each new configuration. However, it is the best approach to do a case study of the flow distribution such as in the boiler heat exchangers.

Sometimes, in boiler heat exchangers, flow non-uniformities occur at both the steam distribution inside the tubes and the combustion products distribution over the tubes. Frequently, these non-uniformities have undesirable effects on the heat exchanger operations such as high gradient temperature at the channels and headers. The operation temperature of boiler tubes is usually high, and the creep rupture is one of the common failures of boiler final superheater and reheat tubes. Creep is a temperature and stress dependent phenomenon, and under a high temperature operation, if the temperature rises 10 K, the creep life of tubes will be reduced to half [22]. Hence, prediction of steam maldistribution and combustion flow maldistribution in the boiler heat exchangers, which cause temperature non-uniformities at the tubes, is very important in design, quality control, and plant evaluations. This paper presents the investigations for the combustion products and

steam flow maldistribution effects on reheat tube rupture in a 250MW boiler using CFD.

2 Power Plant Background

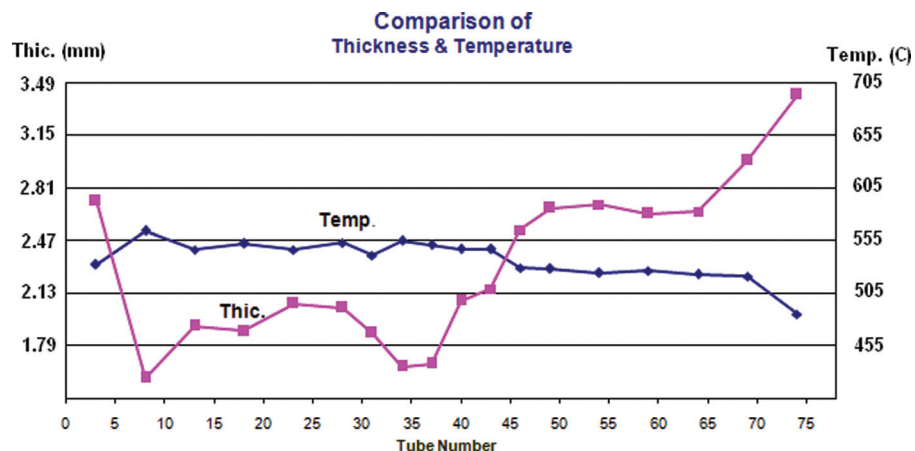
Shahid Rajaee, one of Iran's largest power plants, has four sub-critical 250MW Foster Wheeler boilers. Each of these boilers has 20 burners, and each burner has one central swirling heavy oil injector surrounded by six gas injectors. Each boiler uses a mixture of 16.7 kg/s of Iranian heavy oil and natural gas fuels under full load operation condition. The heat absorption elements have been prepared in three separate Passes inside the boiler as follow: Secondary and final superheater and final reheat elements have been installed in the Pass 1; Pass 2 is the heat recovery area; and Pass 3 is formed by primary and secondary economizer and primary superheater elements. The heat recovery area consists of 76×10 numbers tubes, which have a 38.1 mm inner diameter and are about 65 m in length for each of the tubes connected to headers from both sides. The inlet header feeds the steam to the tubes, and the outlet header gathers the steam for use in the low-pressure turbine. The reheat channels and headers are in U-type configuration. The final reheat tubes' metal, which has non-uniform thinning, is SA-213 TP321H stainless steel with a nominal thickness of 5 mm. Residual life of these tubes was evaluated previously by Poursaeidi et al. [23]; they concluded that the erosion and corrosion rates will increase with increasing in temperature of the tubes.

3 Experimental analysis

Due to observing a non-uniform wall thinning of final reheat tubes, a series of experimental tests were done as follows.

3.1 Temperature Measurements. The temperature of final reheat tubes is recorded with the sensors installed in the header box where the metal temperature is measured regularly. Recorded temperatures are shown in Graph 1. As shown in Graph 1, the temperature of the tubes in left side of the boiler (tubes 1 to around 40) is more than the values corresponding to the right side tubes (tubes about 40–76).

3.2 Thickness Measurements. The thicknesses of the final reheat tubes were measured by an ultrasonic thickness gauge model, ELCOMETER 206 D, in five locations [24]. The comparison of measured final reheat tubes thicknesses after 80,000 h of operation with recorded temperature of these tubes is depicted in Graph 1 [24]. Tubes 1–5 were replaced in the second overhaul (in 2004) and, thus, do not show a correct decrease in thickness. Tubes on the left side (6 to around 40) have decreased in thickness



Graph 1 Comparison of average thickness of reheat tubes with recorded temperature

Table 1 Measured properties for the samples

	Hardness ASTM-384 (HV)	Oxide thickness	Depletion zone Max & Min	Average slag	Total conductivity (W/K.m)	Total specific heat (J/kg.K)	Density (kg/dm ³)
Tube 11 {fireside}	201	138	12 & 6	310	13	505	7.9
Tube 39 {fireside}	191	40	11 & 5	340	12.8	500	7.9
Tube 66 {fireside}	227	28	7 & 4	280	13.1	495	7.9

more than those on the right side, and tubes 6-39 were replaced in the last overhaul (in 2008), which is shown in Fig. 1 [24].

Reheater tubes No. 11, 37, and 66 were chosen to take samples for destructive tests.

3.3 Hardness Test. First, a ring with a parallel surface was cut from each sample of tubes, then the roughness of the surface of the rings was reduced by sand paper of meshes 120-800 and finally the hardness was measured by universal hardness machine model: SWISS-MAX and by HV hardness indenter. Results of hardness test are shown in Table 1.

3.4 Dimension Measurement. A ring was prepared from each sample tube, and then outer and inner diameters and thickness of rings were measured in some direction by caliper. Results are shown in Table 1.

3.5 Metallographic Tests. Two specimens from each sample of tubes (fireside and backside) were prepared. Then these specimens were mounted, ground, polished, and etched. Specimens were inspected by optical microscope as shown in Fig. 2, then inner and outer oxide layer thicknesses, depletion zone, and combustion products thicknesses (slag) were measured as shown in Table 1.

As shown in Fig. 2 and Table 1, hardness of tubes 11 and 37 are lower and their oxide thicknesses and depleted depths are higher than the values for the tube 66. These results show that tubes 11 and 37 were exposed on higher temperature operation than was tube 66. Consequently, high temperature erosion can be assumed to be the most important and obvious factor for thinning of tubes.

4 Governing Equations

CFD modeling finds a numerical solution to the conservation equations. In studies of turbulent flow, the random nature of the flow precludes the use of computation based on a complete description of the motion of all fluid particles. Introducing time-averaged properties of the flow (mean velocity, pressure, and stress) to the time-dependent Navier-Stokes equations leads to the time-averaged Navier-Stokes equations [25]. A turbulence model is required to close the system of mean flow equations so that they can be solved for a wide variety of flow problems. Classical turbulence models include the mixing length, k- ϵ family models, Reynolds-Stress model, and algebraic stress models. For CFD researches, the k- ϵ family models [26] are advantageous because they require less CPU time and cover a wide range of turbulent flows; thus, they were applied in this work.

There are several combustion models to simulate the combustion flows, too. In the boiler that was studied, the combustion is non-premixed model, so this model was used to simulate the combustion. For simulating the radiation heat transfer phenomenon, there are five models available in the FLUENT software. The P-1 radiation model was used in this study [27]. All the models and procedures that are used in FLUENT software to solve a range of fluid mechanics and heat transfer problems are clearly explained in the Fluent 6.3.26 user manual [28].

5 Simulation Results

5.1 Geometric Calculations. The heat recovery tubes are subchannels that have been joined to headers from both sides (so called parallel channels). The inlet header feeds steam to the tubes, and the outlet header gathers the steam. The goal is to sim-

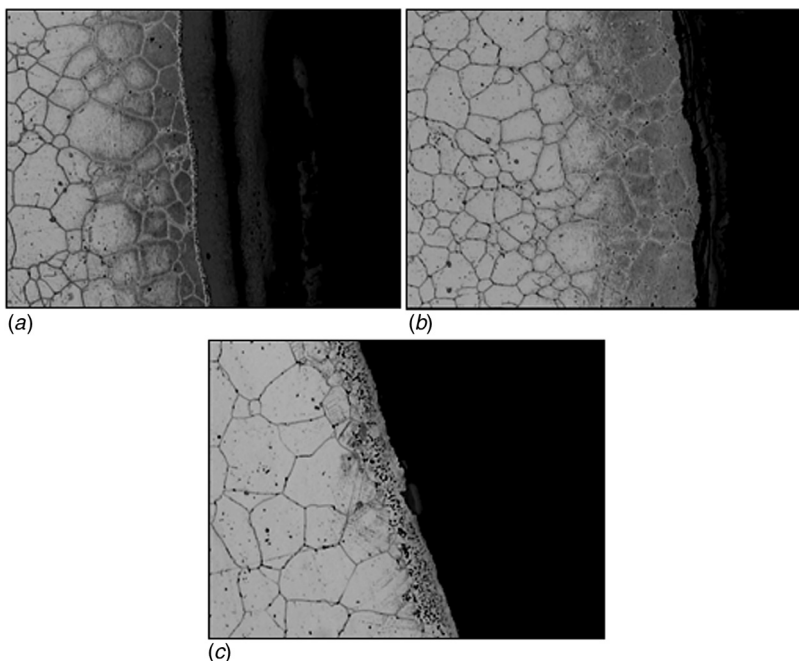


Fig. 2 Metallography for tubes 11 (a), 37 (b), 66 (c)

ulate the steam distribution in the tubes. But the geometry of these tubes and headers is very complex, and without knowledge of flow coefficients, such as the friction and pressure recovery coefficients, they can't be analyzed without CFD codes. On the other hand, because of this complexity and existence of pressure gradient along the headers, periodic and symmetric boundary conditions can't be used for it, so that 3-D simulating of this geometry needs a super-

computer with vast capacity. Thus, 2-D geometry equal with 3-D geometry conditions should be applied for simulating of such complex geometries, and then the results (such as mass flow rate in the channels and static pressure along the headers) can be used to simulate the 3-D geometry of the tubes without headers. The design data for steam flow in heat recovery area under 250 MW thermal power outlet condition are as follows

$$m_{tot} = 192.67 \text{ kg/s}$$

$$T_{out} = 550^\circ\text{C}$$

$$D_{H,out} = 0.66 \text{ m}$$

$$p_{in} = 37.3 \text{ bar}$$

$$\rho_{in} = 37.3 \text{ kg/m}^3$$

$$\mu = 3.137 \times 10^{-5} \text{ Pa.s}$$

$$p_{out} = 34.3 \text{ bar}$$

$$\rho_{out} = 9.17 \text{ kg/m}^3$$

$$D_{H,in} = 0.61 \text{ m}$$

$$V_{t,2-D} = V_{t,R}; \quad V_{t,R} = (m_{t,R}/\rho A_{t,R})$$

$$= 0.253526315/(11 \times 0.000963) = 23.94 \text{ m/s} \quad (7)$$

$$f = 0.25/\{\log[(e/3.7 \times D) + (5.74/Re^{0.9})]\}^2;$$

$$\{500 \leq Re \leq 10^8, 10^{-6} \leq e/D \leq 10^{-2}\} \text{ [Ref. 29]} \quad (8)$$

The goal is to supply 2-D conditions so that average mass flow rate, Reynolds number, and head loss along the reheater headers and tubes become equal with the same values that can be calculated from the design data. The average mass flow rate for each tube under operation condition is as follows

$$m_{t,R} = m_{tot} \div (76 \times 10) = 192.68 \div 760 = 0.253526315 \text{ kg/s} \quad (1)$$

Head loss for real condition is calculated as follows

$$H_{loss} = (\Delta P \div \rho_{av}) - (g \times \Delta z) = (300000 \div 11) - (20 \times 9.81) \approx 27092.38 \text{ (m/s)}^2 \quad (2)$$

The average Reynolds number for flow in the tubes under real condition is as follows

$$Re = \rho V D / \mu \rightarrow Re_{t,R} = 320000$$

→ Thus the flow is turbulent inside the tubes (3)

For simulation, the mass flow rate is considered constant, and each tube under 2-D condition is equal with 10 tubes in a row under real conditions. The diameter and length of each tube for 2-D geometry are calculated as follows

$$m_{t,2-D} = \rho V D = m_{t,R} \times 10 = 2.53526315 \text{ kg/s} \quad (4)$$

$$Re_{t,2-D} = \rho V D / \mu = m_{t,2-D} / \mu_{2-D};$$

$$Re_{t,2-D} = Re_{t,R} = 320000.$$

$$\rightarrow \mu_{2-D} = 7.9227 \times 10^{-6} \text{ Pa.s} \quad (5)$$

$$H_{loss} = f \times (L/D)(V^2/2) \quad (6)$$

Granted that: $e/D = 0.01 \rightarrow f = 0.038204214$

$$L/D = (2 \times H_{loss}) / (f \times V^2)$$

$$= (2 \times 27092.38) / (0.038204214 \times 23.94^2)$$

$$= 2474.6 \quad (9)$$

Now there is a reciprocal equation between length and diameter of tubes. So it is granted that

$$D_{t,2-D} = 0.01(m) \rightarrow L_{t,2-D} = 24.746 \text{ m}$$

Now by considering that the average velocity of flow in 2-D headers should be equal with the average velocity of flow in real headers, the diameter of header is calculated as follows

$$D_{H,R} = 0.61 \text{ m} \rightarrow A_{H,R} = (\pi \times D_{H,R}^2)/4 = 0.093025 \pi \text{ m}^2 \quad (10)$$

$$m_{tot} = \rho_{av} \times V_{H,R} \times A_{H,R} = 192.68 \text{ kg/s} \rightarrow V_{H,R} = 59.95 \text{ m/s} \quad (11)$$

$$m_{tot} = m_{H,2-D} = \rho_{av} \times V_{H,2-D} \times D_{H,2-D} = 192.68 \text{ kg/s}$$

$$\rightarrow D_{H,2-D} = 0.292 \text{ m} \quad (12)$$

5.2 Combustion Simulation. To demonstrate fuel characteristics, Tables 2 and 3 [30] show natural gas and heavy oil, respectively, analysis for the Shahid Rajae power plant boiler. FLUENT software was used to simulate combustion, fluid and

Table 2 Natural gas fuel analysis

Component	H2S (ppm)	N2	C1	CO2	C2	C3	IC4	NC4	IC5	NC5	C6	NCV	GCV
ASTM-1945 Standard Value (mol %)	3.6	4.7	88.7	0.6	4.3	1.08	0.2	0.27	0.08	0.05	0.02	-	
CIP Standard Value (MJ/m3)	-	-	-	-	-	-	-	-	-	-	-	34.4	38.1

Table 3 Heavy oil fuel analysis

Component	C	H	O	S	ASH	V	Na	Ni	Pb	Ca	LCV	HCV
Value (mass %)	85.05	10.25	1.82	2.88	0.02	-						
Value (ppm)	-	-	-	-	-	65	21.4	17.4	0.3	2.6	-	
Value (kCal/kg)											9798.7	10290.83

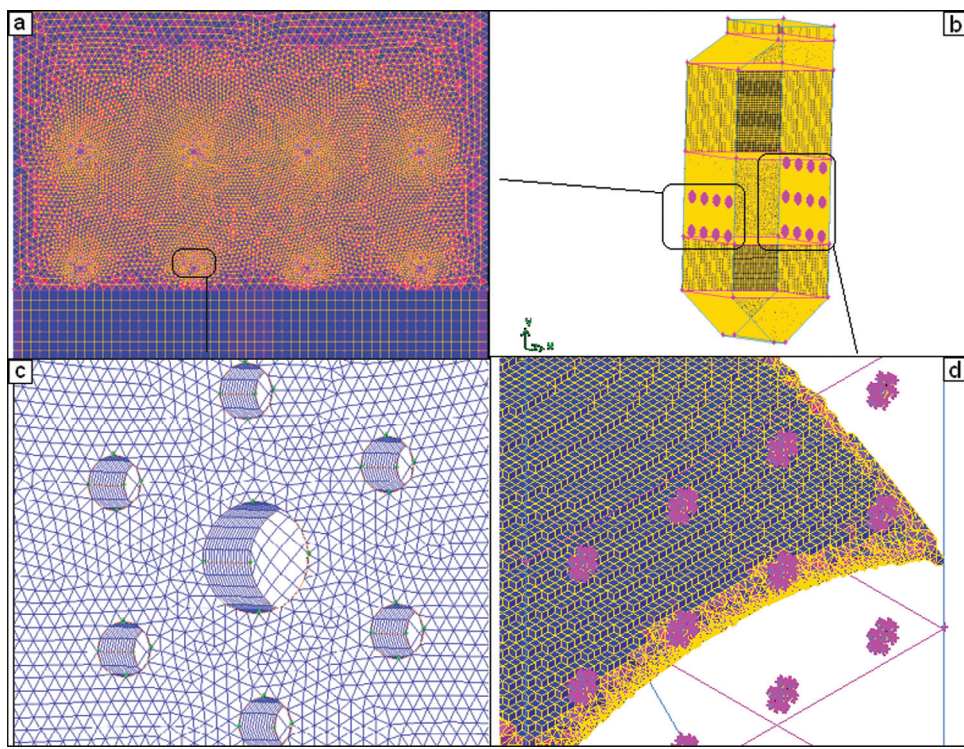


Fig. 3 Combustion chamber meshes

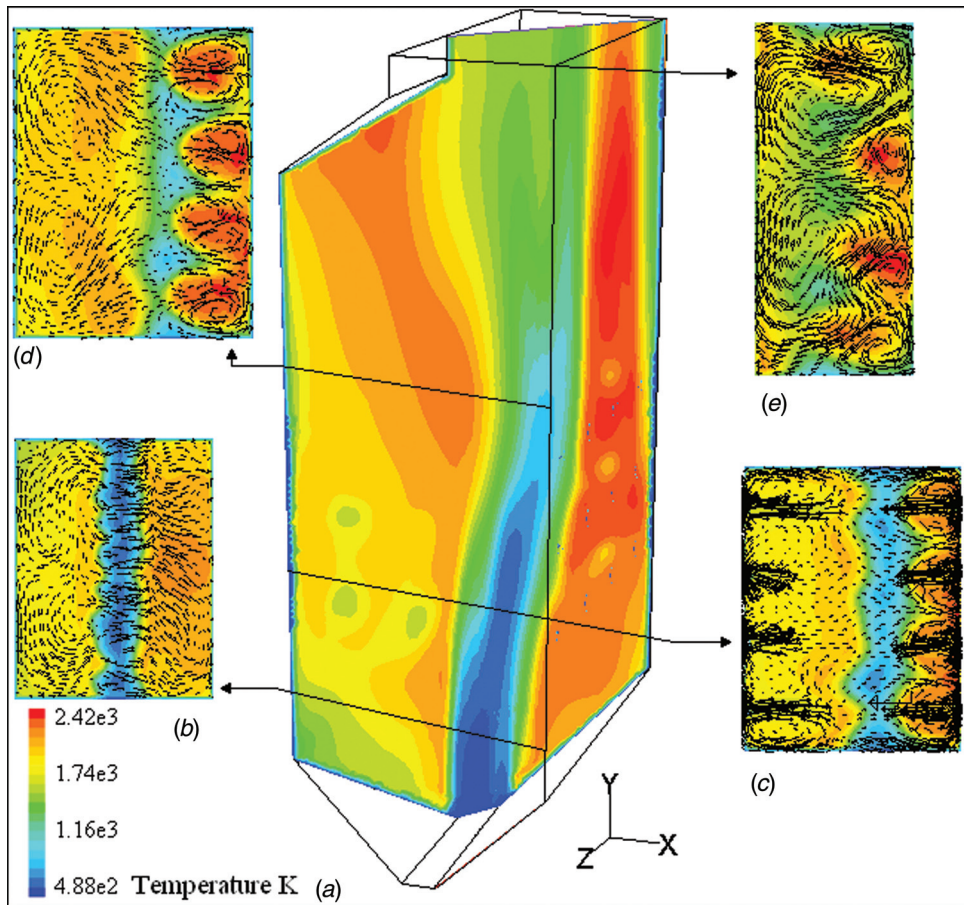


Fig. 4 (a) Temperature field; (b) to (e) Temperature of horizontal planes at positions indicated by the arrows

Table 4 Consistency of simulation results

	Operation load	Excess air (%)	SO ₂ (ppm)	NO _x (ppm)	CO (ppm)	HC (ppm)	CO ₂ (%)	O ₂ (%)	Sec. S.H. heat transfer rate (kW/m ²)	F. S.H. heat transfer rate (kW/m ²)
Experimental data	168-MW	50.1	1670	272	24	0	10.9	1.63	71.6	32.15
Experimental data	171-MW	54	1824	406	8	0	10.89	1.78	72.5	32.56
Simulation data	150-MW	55	1483	229	31	0	11.31	2.82	68.3	33.39
Simulation data	200-MW	72	1437	356	27	0	10.65	5.76	90.2	44.71
Simulation data	250-MW	94	1391	460	16	0	9.92	7.8	116.6	56.62

particle flow, heat, and mass transfer inside the furnace. Boiler geometry was modeled downstream up to the beginning of Pass 1. First of all, the boiler geometry was covered with three different meshes (749,983, 883,857, and 1,065,790 cells), and a parametric analysis was accomplished to confirm whether or not numerical results were grid independent. After determining mesh independency, the medium size mesh (883,857 cells) was chosen for the different conditions simulations. Mesh density was refined in the neighborhood of fuel and air inlet sections, being progressively decreased inside the furnace.

A non-premixed combustion model [28] was used to simulate the furnace under three different operation load conditions (60%, 80%, and 100% of full load). The non-premixed combustion model needs a PDF table to calculate the reactions and their properties in the simulations. In fact, in FLUENT software, the mixture fraction and its variance are solved instead of reaction equations, and the reaction equations are solved in PrePDF software. The PrePDF software calculates the combustion reactions according to the mixture fractions (the mixture fractions depends on equivalence ratio) and produces the PDF tables for using in the FLUENT software. In other words, the PDF tables consist of thermochemistry information.

To calculate the fields of velocity, temperature, and concentration of species, the discretized conservation equations for mass, momentum, and energy were solved in the FLUENT software. Flow was assumed to be stable, and the segregated solver was used because instability of every conservation equation does not affect other equations' stabilities. Turbulence closure is achieved

by means of the standard $k-\epsilon$ model. The P-1 radiation model was used to calculate the radiative heat transfer to and from the combustion species and waterwalls. For boundary conditions, mass flow rates, temperatures, and mixture fractions were fixed on the inlet sections, and non-equilibrium wall functions were used at solid walls [28]. According to the amount of water that is converted to vapor along the waterwalls, the heat flux on the walls of the chamber was calculated. Then the constant value of heat flux was imposed on the enclosure walls: 116.2 kW/m², and the roughness of walls was also set: 0.05. The pressure outlet condition was chosen for outlet boundary, and the gage pressure was set to zero.

Because loading of heavy oil particles (dispersed phase loading) to the gas and air mixture (continuum carrier phase) was less than 0.001, the discrete phase model was used to handle the multiphase problem [31]. In the boiler studied, the heavy oil injectors are of the air-blast type while the tips of these injectors are of the swirling type to do best atomization. In the simulation, the air-blast atomization type was used. The discrete random walk model was used for stochastic tracking of droplets. Thermal conductivity, viscosity, absorption coefficient model, and scattering coefficient of mixture were set to 0.025 W/m.K, 2×10^{-5} kg/m.s, wsgm-cell-based [28] and zero, respectively.

The gas phase homogeneous combustion has been modeled using the equilibrium hypothesis with applying rich flammability limits to evaluate the non-equilibrium reactions as a partial equilibrium model [28]. Instantaneous mass fractions are determined in terms of the instantaneous mixture fraction. Mean mass fractions of fuel, oxidizer, and products are obtained from the mean

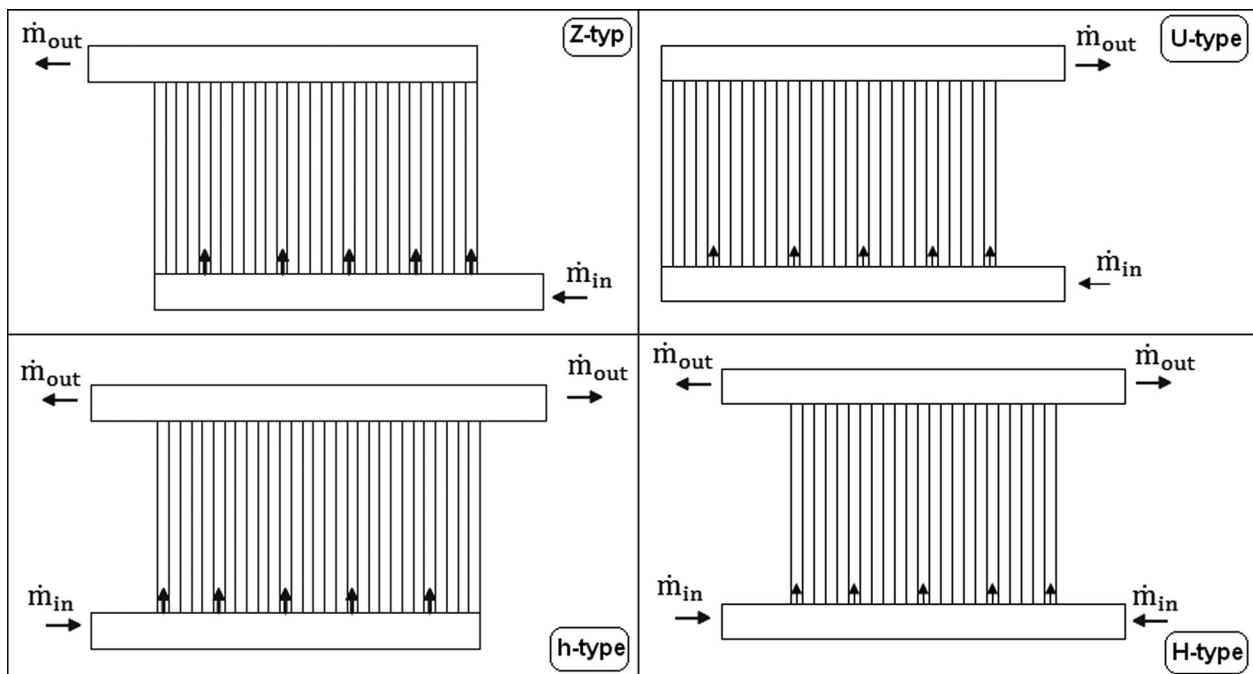
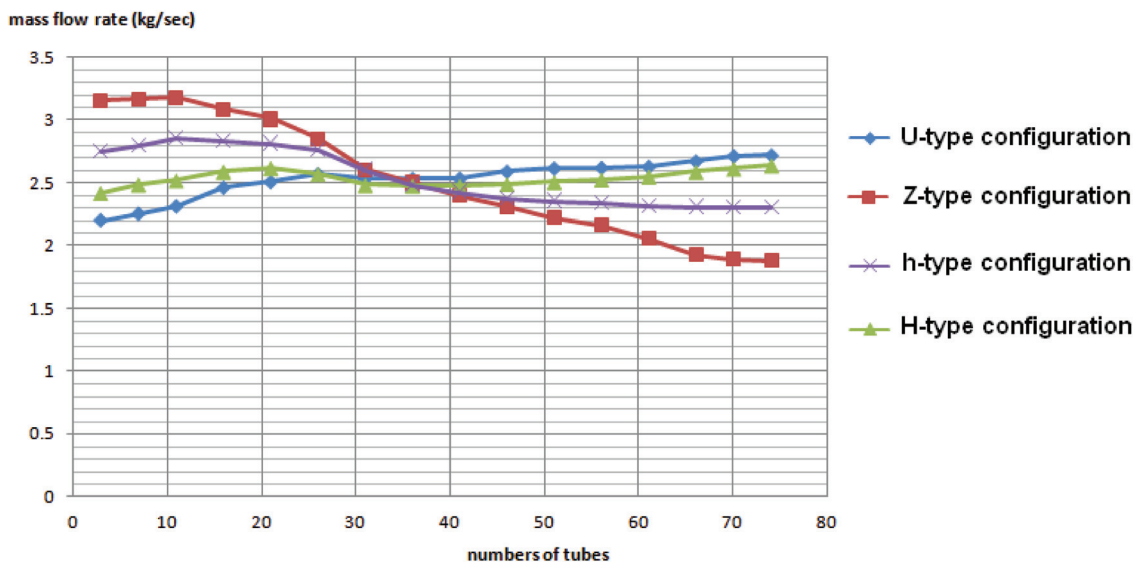


Fig. 5 Schematic of various configurations of parallel channels



Graph 2 Mass flow distribution in the reheat tubes for various configuration parallel channels

and variance of instantaneous values, assuming a β -PDF distribution [28]. For pressure-velocity coupling, the SIMPLE method was used, and the second order upwind differential scheme was employed to approximate the convective terms. The solutions were considered to be converged when the sum of the normalized residuals for each control equation was of order of 1×10^{-6} . Figure 3 shows the arrangement of the burners [Fig. 3(a)], meshed geometry [Fig. 3(b)], burner geometry [Fig. (c)], and quality of the meshes inside the chamber [Fig. 3(d)].

The temperature distribution for a vertical plane diagonally positioned is shown in Fig. 4(a). The temperature and velocity

fields are presented in a superimposed way in Figs. 4(b) to 4(e) for horizontal planes corresponding to the downstream burner level, secondary burner level, upstream burner level, and a level exactly in the entrance of the Pass 1. The main control parameters used to validate the combustion simulation results were the temperature and mass fractions of gases in the boiler outlet. These are measured regularly [30]. Table 4 shows the main results consistency.

As it is shown in Table 4, the simulation results are in good agreement with the operation data. Furthermore, simulation gives the average temperature 1682 K at the chamber outlet under 250

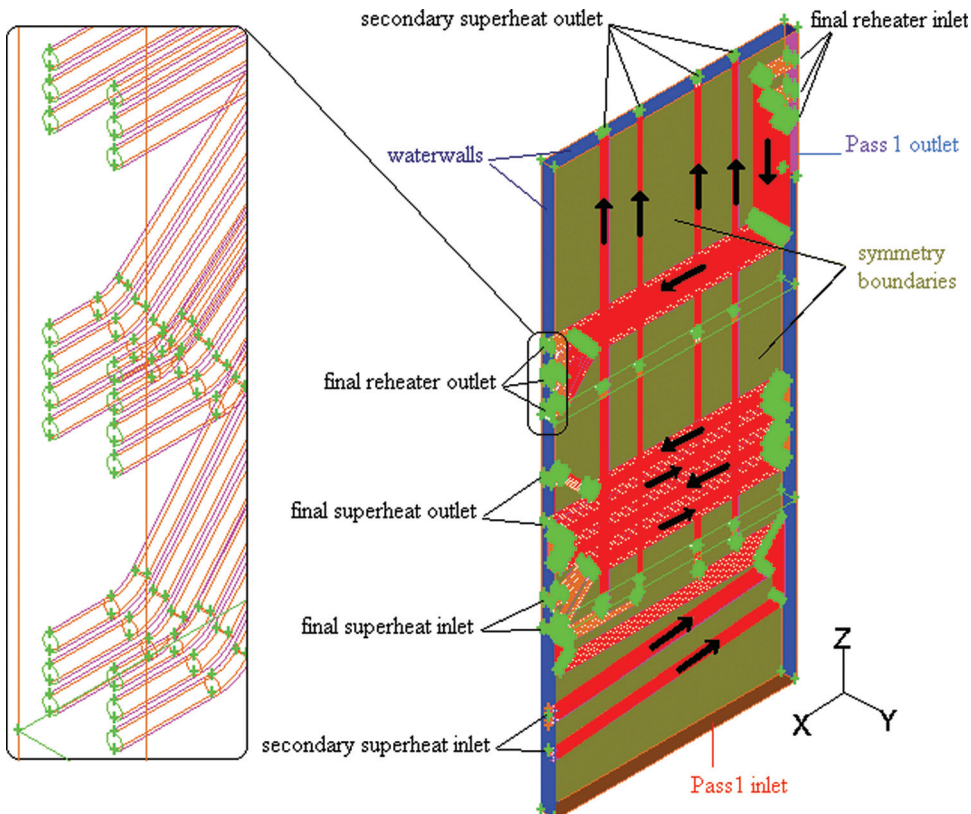


Fig. 6 Geometry of heat exchangers inside Pass 1

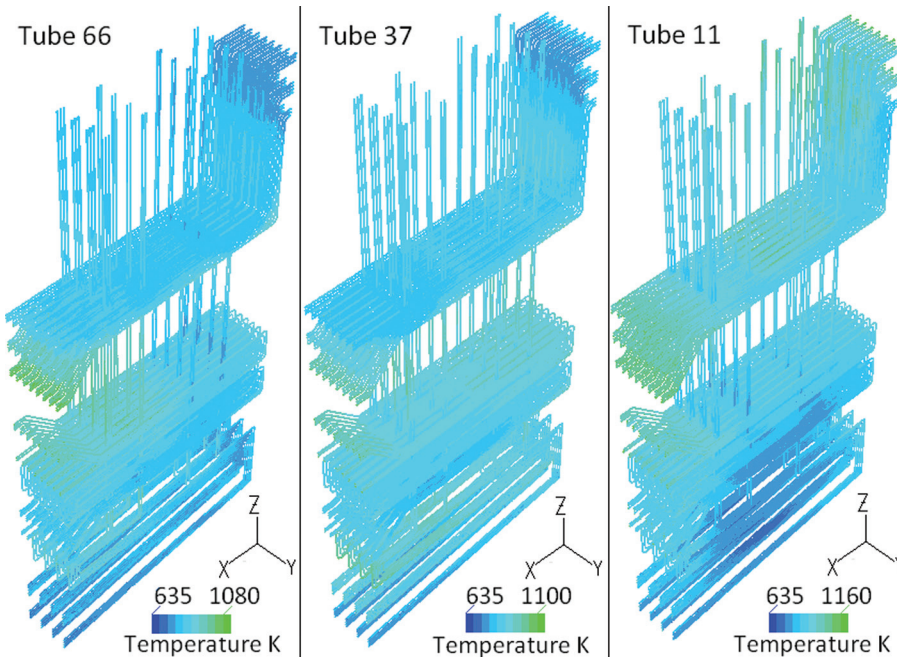


Fig. 7 Temperature distribution for the reheat tubes 11, 37, and 66

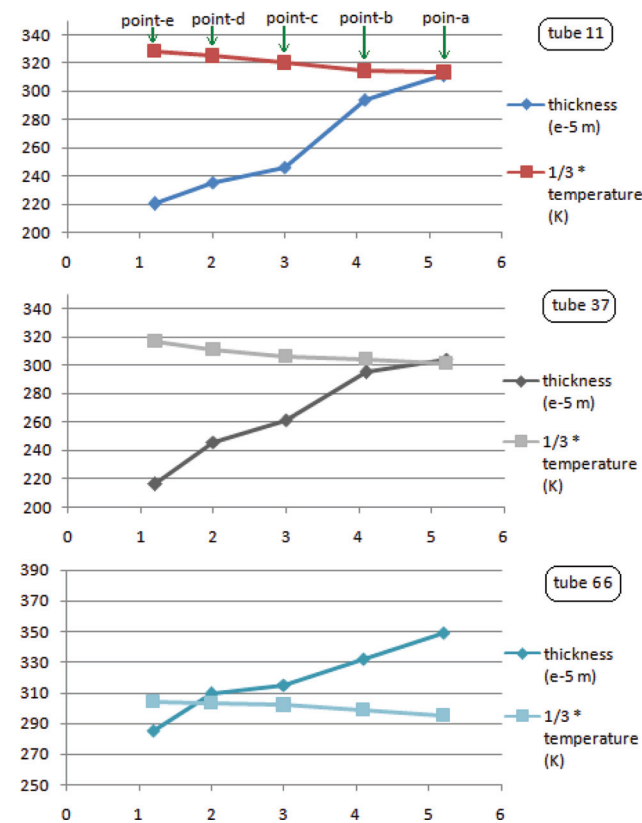
MW operation; this is in good agreement with the value from the design information of 1687 K.

5.3 Mass Flow Distribution in the Reheater Tubes. The 2-D geometry of headers and tubes were constructed with Gambit software according to the geometry parameters calculated in Sec. 5.1. Constructive quadrilateral grids were applied to mesh the geometry, and the number of the involved cells was 750,000. By assuming that the channel surface roughness parameter is 0.01, the fluid (water vapor) is compressible and the flow pattern is stable, the flow in the tubes and headers were simulated by FLUENT software. The standard $k-\epsilon$ model was adopted because the flow was fully turbulent, and furthermore this turbulence model has advantages for simulating lattice geometries in comparison with other turbulent models available in FLUENT software. The non-equilibrium wall function was chosen for near-wall treatment. To converge the equations, the coupled implicit [28] method was used, and after 30 repeating loops, the Courant number increased to 50. In the simulation, on the inlet boundaries, the mass flow rate was the input, and all the outlets were defined as outflow boundary condition. On all solid surfaces, the no-slip wall boundary condition was imposed. The solution was considered to be converged when the sum of the normalized residuals for each control equation was of order of 1×10^{-6} .

Four various types of parallel-channel configuration (U-, Z-, h- and H-types) were simulated with the boundary conditions for these configurations being shown in Fig. 5. For U-type [Fig. 5(a)], Z-type [Fig. 5(b)], and h-type headers [Fig. 5(c)], steam feeds from one side of inlet header and offloads from the same side, opposite side, and both sides at outlet header, respectively. For these configurations, non-uniform feeding and offloading of headers increase the pressure gradient along the headers but this non-uniformity decreases for H-type headers [Fig. 5(d)] due to square sides feeding and offloading. Results of flow distribution simulation for the mentioned configurations of headers are shown in Graph 2.

5.4 Pass 1 Heat Exchangers Simulation. The Pass 1 of the boiler consists of a 38×9 secondary superheater, a 76×10 final superheater, and reheater thermal elements. In this simulation, the 3-D geometry of the 2×10 elements of final superheater and

reheater and 1×9 elements of secondary superheater tubes inside the boiler were constructed with Gambit software according to the tubes geometry parameters. Unstructured hybrid tetrahedral/prism grids were used to mesh the geometry. The number of the involved cells was 1,205,980. Figure 6 shows the geometry and applied boundaries. All the solids surface roughness parameter is



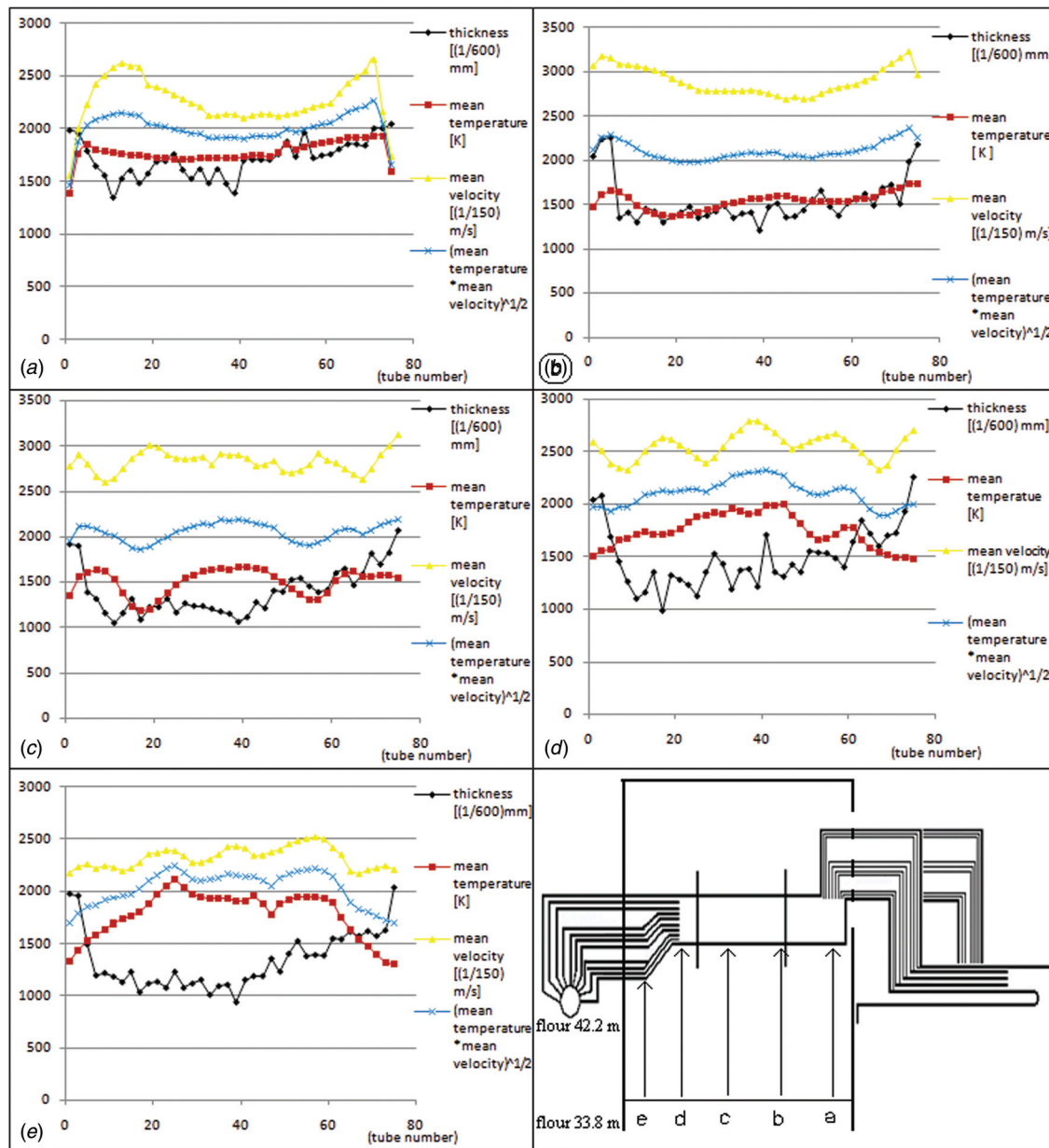
Graph 3 Comparison of measured thickness with calculated temperature gradient in tubes axial direction for reheat tubes 11, 37, and 66

0.05, and the flow pattern is assumed to be stable. The tubes 11, 37, and 66 were chosen for simulating heat transfer from combustion products to the steam flowing in the tubes. The mass flow boundary conditions for tubes 11, 37, and 66 were set according to the amount of steam flow in them under U-type configuration, which was simulated in Sec. 5.3. The outlet chamber in the combustion simulation geometry was divided into 38 parts, and flow properties such as velocity, density, pressure, thermal conductivity, heat capacity, and turbulence parameters were written to a profile and then the parts that correspond to tubes 11, 37, and 66 were set as boundary condition properties in Pass 1 simulation.

According to our experience on CFD modeling, the realizable k- ϵ model has more advantages for heat exchanger simulations in comparison with other turbulence models, so this model was used in this simulation. The enhanced wall treatment was chosen for the near-wall treatment due to a need for a high degree of accuracy in the turbulent and viscous layers, which are affected by means of tubes inside the boiler. For pressure-velocity coupling, the SIMPLE method was used, and the second order upwind dif-

ferential scheme was employed to approximate the convective terms. All the outlets were defined as pressure outlets. On the waterwalls surfaces, a no-slip wall boundary condition and on other couple vertical surfaces symmetric boundary conditions were imposed. The amount of average heat transfer in the boiler waterwalls was set to the wall heat flux boundary condition on waterwalls boundaries, and the measured thickness and conductivity were set for the tube boundaries. The solution was considered to be converged when the sum of the normalized residuals for each control equation was of order of 1×10^{-6} .

The temperature distribution for the reheater tubes are shown in Fig. 7. The comparison of temperature gradient for three simulated tubes with their measured thickness in tubes axial direction (X direction) [24] is depicted in Graph 3. As shown in Graph 3, the non-uniform tube thickness decrease in the tubes' axial direction is proportional to the non-uniformity of these tubes temperature. Simulations give the mean temperature of final reheat tubes 11, 37, and 66 to be 960, 917, and 905 K in the outer side and 904, 851, and 850 K in inner side, respectively. So the



Graph 4 Comparison of the average temperature and velocity of 3 operation conditions for 5 directions with measured tube thicknesses in the directions

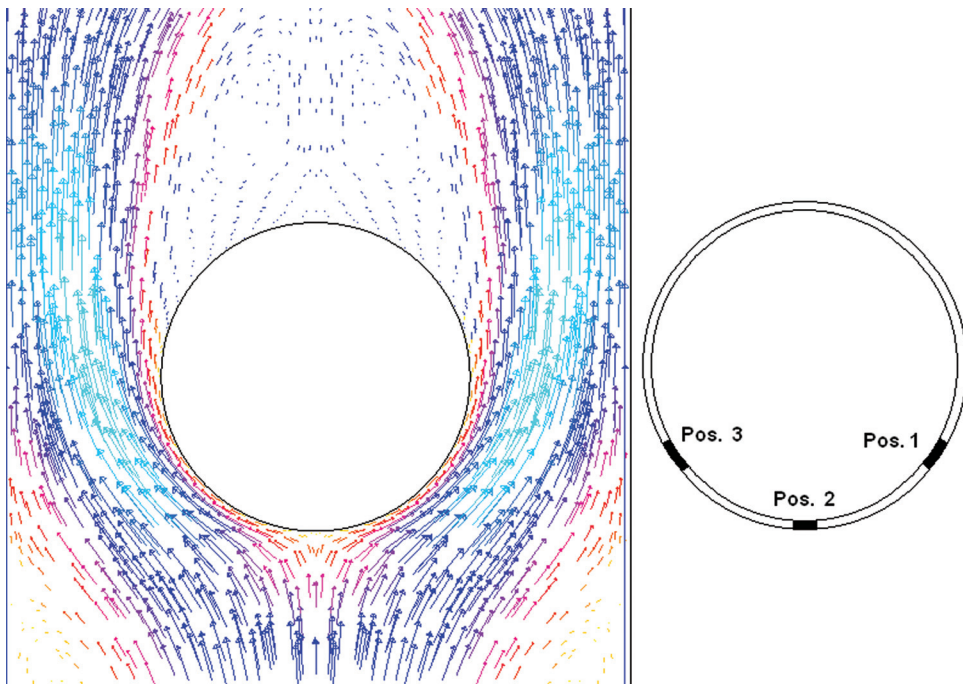


Fig. 8 Velocity vectors and positions around the tubes for which thicknesses are measured

temperature of reheater tubes in the left side of boiler is more than that of the tubes on the right side.

For validating the heat transfer simulation in the heat exchangers, the heat transfer rate from the combustion products to the steam flowing in the tubes was calculated and compared with the simulation results which are shown in Table 4. As shown in Table 4, simulation results are in good agreement with the operation data. Also a comparison of temperature gradient in the tubes' axial direction by measured thickness in Graph 3 shows the accuracy of the temperature distribution results.

6 Conclusions

Final reheat tube thickness measurements showed non-uniformity in these tubes. Experimental analysis showed that final reheat tubes were exposed to high temperature distribution in the left side of the boiler, and tubes thicknesses on this side are reduced more than the other side. Non-uniform temperature distributions can have two possible reasons, problems due to combustion and to steam distribution in the tubes. Therefore combustion in the boiler chamber, steam flow distribution in the reheat tubes, and heat transfer in Pass 1 heat exchangers were simulated using FLUENT software.

6.1 According to Combustion Simulation Results. The amount of mean temperature and velocity in five important locations at the chamber outlet (locations for which tube thicknesses are measured [24]) for operation at 250, 200, and 150 MW are calculated from combustion simulation results. Graph 4 compares the mean temperature and velocity of combustion products for three operation conditions for five mentioned locations with measured tube thicknesses. According to Graph 4, the temperature distribution non-uniformity is clearly shown at the chamber outlet. This is due to poor design, but this non-uniformity is not proportional to the decrease in non-uniform reheat tube thickness. According to the measurements [24], the thicknesses of tubes in positions 1 and 3 are less than the value for position 2 at the same point as shown in Fig. 8. This is due to the high amount of combustion product flow velocity in positions 1 and 3 that causes high frictional erosion. Furthermore, the tube thinning rate in high temperature areas is more than the values that correspond to the lower

temperature regions. Therefore by assuming that high temperature and frictional erosions have the same order effect on tube thinning, the parameter $(\text{mean temperature} \times \text{mean velocity})^{1/2}$ will be a good gauge to assess the effects of combustion products on the tube thinning rates because this parameter applies the effects of frictional and high temperature erosions together. As shown in Graph 4, a comparison of the parameter $(\text{mean temperature} \times \text{mean velocity})^{1/2}$ with the tube thicknesses shows that the tube thinning is not proportional to the combustion product distribution on the tubes. These results show that tube thickness non-uniformity is not due to combustion products distribution on the tubes.

6.2 According to Simulation of Steam Flow Distribution in Reheater Tubes. Four various types of parallel-channel configuration (U-, Z-, h- and H-type) were simulated. Results of flow distribution simulation for the mentioned configurations of headers are shown in Graph 2. As shown in Graph 2, the distribution of mass flow in the tubes under designed condition (U-type header) is not uniform, so that the average mass flow rate in tubes closer to the feeding side (right side of the boiler) is more than those values for tubes that are far from the feeding side of headers (left side of the boiler). The variation of mass flow rate in tubes 76 down to around 40 under the designed condition is not sensible, but after tube 40 down to 1, the mass flow rate suddenly decreases. These results exactly show the reason of non-uniform tube thickness decreasing, which is shown in Graph 1. By comparing of steam flow distribution for various simulated configuration headers, it can be concluded that the H-type header has more uniform flow distribution than the other types.

6.3 According to Pass 1 Heat Exchanger Simulation. Simulations give the average temperature of final reheat tubes 11, 37, and 66 to be 960, 917, and 905 K in the outer side and 904, 851, and 850 K in the inner side, respectively. As shown in Graph 2, the non-uniform tube thickness decreasing in the tubes' axial direction is proportional to the non-uniformity of these tubes' temperature. By comparing Graphs 1 and 2 and by considering the amount of calculated average temperature for the three mentioned tubes, it can be concluded that a further decrease

in thickness of tubes 1 to around 40 results from mal-distribution of steam flow in the tubes. In addition, it is shown that the mass flow distribution for an H-type header is more uniform than the other types. Therefore for making the steam flow distribution and the temperature distribution in final reheatertubes more uniform and decreasing the non-uniformity of these tubes thinning the H-type headers is the best choice.

Nomenclature

A	= area (m^2)
D	= diameter of tube (m)
e/D	= roughness ratio
f	= friction factor
GCV	= gross calorific value
HCV	= higher calorific value
H_{loss}	= head loss (m)
k	= conductivity
L	= length of tube (m)
LCV	= lower calorific value
m	= mass flow rate (kg/s)
NCV	= net calorific value
ρ	= density of steam (kg/m^3)
δ	= thickness (mm)
μ	= viscosity (pa.s)
3-D	= 3-dimensional
2-D	= 2-dimensional

Subscript

av	= average of outlet and inlet steam value
H	= header
in	= reheater inlet header steam value
out	= reheater outlet header steam value
R	= real condition
t	= tube
tot	= total

References

- [1] Chiou, J. P., 1978, "Thermal Performance Deterioration in Crossflow Heat Exchanger Due to the Flow Nonuniformity," *ASME J. Heat Transfer*, **100**, pp. 580–587.
- [2] Shah, R. K., and London, A. L., 1980, "Effects of Nonuniform Passages on Compact Heat Exchanger Performance," *J. Eng. Power*, **102**, pp. 653–659.
- [3] Lalot, S., Florent, P., Lang, S. K., and Bergles, A. E., 1999, "Flow Mal-Distribution in Heat Exchangers," *Appl. Thermal Eng.*, **19**(8), pp. 847–863.
- [4] Tondeur, D., and Luo, L. A., 2004, "Design and Scaling Laws of Ramified Fluid Distributors by the Constructal Approach," *Chem. Eng. Sci.*, **59**(8–9), pp. 1799–1813.
- [5] Luo, L. A., and Tondeur, D., 2005, "Optimal Distribution of Viscous Dissipation in a Multi-Scale Branched Fluid Distributor," *Int. J. Therm. Sci.*, **44**(12), pp. 1131–1141.
- [6] Luo, L. A., and Tondeur, D., 2005, "Multiscale Optimization of Flow Distribution by Constructal Approach," *China Particul.*, **3**(6), pp. 329–336.
- [7] Luo, L. A., Fan, Y. L., Zhang, W. W., Yuan, X. G., and Midoux, N., 2007, "Integration of Constructal Distributors to a Mini Crossflow Heat Exchanger and Their Assembly Configuration Optimization," *Chem. Eng. Sci.*, **62**(13), pp. 3605–3619.
- [8] Luo, L. A., Fan, Z. W., Le Gall, H., Zhou, X. G., and Yuan, W. K., 2008, "Experimental Study of Constructal Distributor for Flow Equidistribution in a Mini Crossflow Heat Exchanger (MCHE)," *Chem. Eng. Process.*, **47**(2), pp. 229–236.
- [9] Yuan, J., Rokni, M., and Sunsen, B., 2001, "Simulation of Fully Developed Laminar Heat and Mass Transfer in Fuel Cell Ducts with different Cross-Sections," *Int. J. Heat/Mass Transfer*, **44**, pp. 4047–4058.
- [10] Jiao, K., Zhou, B., and Quan, P., 2006, "Liquid Water Transport in Straight Micro-Parallel-Channels with Manifolds for PEM Fuel Cell Cathode," *J. Power Sources*, **157**, pp. 226–243.
- [11] Jung, H. M., Lee, W. Y., Park, J. S., and Kim, C. S., 2004, "Numerical Analysis of a Polymer Electrolyte Fuel Cell," *Int. J. Hydrogen Energy*, **29**(9), pp. 945–954.
- [12] Chen, C. H., Jung, S. P., and Yen, S. C., 2007, "Flow Distribution in the Manifold of PEM Fuel Cell Stack," *J. Power Sources*, **173**(1), pp. 249–263.
- [13] Mohan, G., Roa, B. P., Das, S. K., Pandiyam, S., Rajalakshmi, N., and Dhathathreyan, K. S., 2004, "Analysis of Flow Mal-Distribution of Fuel and Oxidant in a PEMFC," *ASME J. Energy Resour. Technol.*, **126**, pp. 262–270.
- [14] Kapadia, S., and Anderson, W. K., 2009, "Sensitivity Analysis for Solid Oxide Fuel Cells Using a Three-Dimensional Numerical Model," *J. Power Sources*, **189**(2), pp. 1074–1082.
- [15] Boersma, R. J., and Sammes, N. M., 1996, "Computational Analysis of the Gas Flow Distribution in Solid Oxide Fuel Cell Stacks," *J. Power Sources*, **63**(2), pp. 215–219.
- [16] Chang, P. A. C., St-Pierre, J., Stumper, J., and Wetton, B., 2006, "Flow Distribution in Proton Exchange Membrane Fuel Cell Stacks," *J. Power Sources*, **162**, pp. 340–355.
- [17] Koh, J. H., Seo, H. K., Lee, C. G., Yoo, Y. S., and Lim, H. C., 2003, "Pressure and Flow Distribution in Internal Gas Manifolds of a Fuel Cell Stack," *J. Power Sources*, **115**, pp. 54–65.
- [18] Kee, R. J., Korada, P., Walters, K., and Pavol, M., 2002, "A Generalized Model of the Flow Distribution in Channel Networks of Planar Fuel Cells," *J. Power Sources*, **109**, pp. 148–159.
- [19] Mahardrayya, S., Jayanti, S., and Deshpande, A. P., 2005, "Flow Distribution and Pressure Drop in Parallel-Channel Configurations of Planar Fuel Cells," *J. Power Sources*, **144**, pp. 94–106.
- [20] Junye, W., 2008, "Pressure Drop and Flow Distribution in Parallel-Channel Configurations of Fuel Cells: U-Type Arrangement," *Int. J. Hydrogen Energy*, **33**, pp. 6339–6350.
- [21] Junye, W., 2010, "Pressure Drop and Flow Distribution in Parallel-Channel Configurations of Fuel Cells: Z-Type Arrangement," *Int. J. Hydrogen Energy*, **35**, pp. 5498–5509.
- [22] Viswanathan, R., 1995, *Damage Mechanisms and Life Assessment of High-Temperature Components*, 3rd ed., ASM International, Metals Park, OH, Chaps. 3–5.
- [23] Pouraeidi, E., and Alimadadi, M., 2008, "Utilizing the Monte Carlo Simulation in Life Evaluation of Superheater Tubes," ICME, Johor Bahru, Malaysia 21–33 May.
- [24] Pouraeidi, E., 2006, "Remaining Life Evaluation of Boiler and Turbine Critical Components of Shahid Rajaee Powerplant- Unit 1 (report for the Shahid Rajaee powerplant)," Shahid Rajaee Powerplant, Archives, Qazvin, Iran.
- [25] Versteeg, H. K., and Malalasekera, W., 1995, *An Introduction to Computational Fluid Dynamics the Finite Volume Method*, Pearson Education Limited, Harlow, England.
- [26] Launder, B. E., and Spalding, D. B., 1972, *Lectures in Mathematical Models of Turbulence*, Academic Press, London, UK.
- [27] Siegel, R., and Howell, J. R., 1992, *Thermal Radiation Heat Transfer*, Hemisphere Publication, Washington DC.
- [28] FLUENT, Fluent Inc., 2007, FLUENT 6.3.26 User Manual.
- [29] Swamee, P. K., and Jain, A. K., 1976, "Explicit Equations for Pipe-Flow Problems," *J. Hydraulics Div.*, **102**(5), pp. 657–664.
- [30] Niroo Research, Metallurgical and Chemical Center, Fuel and Oil Lab, 2006, Report No. CF850084, Iran.
- [31] Crowe, C., Sommerfield, M., and Tsuji, Y., 1998, *Multiphase Flows with Droplets and Particles*, CRC Press, Boca Raton, FL.